JOURNAL OF GEOPHYSICAL RESEARCH, VOL. 114, A09107, doi:10.1029/2009JA014346, 2009

Cosmic ray intensity increases detected by Aragats Space Environmental Center monitors during the 23rd solar activity cycle in correlation with geomagnetic storms

A. Chilingarian[1] and N. Bostanjyan[1]

Received 14 April 2009; revised 3 June 2009; accepted 24 June 2009; published 30 September 2009.

[1] Interplanetary coronal mass ejections (ICMEs) dominate the intense geomagnetic storm (GMS) occurrences, and simultaneously, they are correlated with the variations of the spectra of particles, ranging from the isothermal solar wind ions to GeV energy protons and fully stripped nuclei. The aim of this paper is to get more insight in the correlations of the ICME parameters with geospace parameters, including the *Dst* index and the secondary cosmic ray flux. Our observations of GMS occurring during the 23rd solar activity cycle demonstrate that the count rate increase during GMS occurs coherently (or up to 1 h in advance) with *Dst* changes. We show that the ratio between the increases of neutron and charged fluxes is approximately constant in a large range of the GMS severity (−470 to 20 nT). The neutron flux always undergoes larger changes compared to the charged component. The difference in peak amplitude can be explained by the fact that lower-energy primary particles produce neutrons compared to the primaries that generate electrons and muons reaching the Earth's surface. We also illustrate that the main driver of GMS is the southward B_z component of the magnetic field of the ICME. Thus the information on the flux changes for different secondary particles helps to "test" the models of the interplanetary magnetic field and the magnetosphere for understanding of the level of disturbance and the specific mechanisms leading to cutoff rigidity reduction.

Citation: Chilingarian, A., and N. Bostanjyan (2009), Cosmic ray intensity increases detected by Aragats Space Environmental Center monitors during the 23rd solar activity cycle in correlation with geomagnetic storms, *J. Geophys. Res.*, *114*, A09107, doi:10.1029/2009JA014346.

1. Introduction

[2] Huge magnetized plasma clouds and shocks initiated by coronal mass ejections (CME) travel in the interplanetary space with mean velocities up to 2500 km/s. These so-called interplanetary coronal mass ejections (ICMEs) are known as major drivers of severe space weather conditions when arriving at the Earth. On their way to Earth, ICMEs also "modulate" the flux of galactic cosmic rays (GCRs) introducing anisotropy and changing the energy (rigidity) spectra [*Dvornikov et al.*, 1988] of the previously isotropic population of protons and stripped nuclei accelerated in the numerous galactic sources. Changes in the rather stable flux of GCRs are detected by space-borne spectrometers (rigidities up to ∼1 GV) and by world-wide networks of particle detectors (rigidities up to ∼100 GV) located at different latitudes, longitudes, and altitudes.

[3] The magnetic field found in some ICMEs, known as magnetic clouds, usually has a well-formed flux rope structure [see *Koskinen and Huttunen*, 2006, and references therein]. The cross section of the magnetic "rope," a twisted bundle of magnetic fields connecting the Earth's magnetosphere directly to the Sun, was observed by the Time History of Events and Macroscale Interactions during Substorms satellites on 20 May 2007 (see http://science.nasa.gov/headlines/y2007/11dec_themis.htm). This structure can explain the "collisionless" transport of solar cosmic rays via "highways" inside the magnetic system connecting the Sun with ICMEs [see *Valtonen*, 2007, and references therein].

[4] The ICME is a major modulating agent, interacting with GCRs, and introducing anisotropy in their flux. These anisotropies of GCRs manifested themselves as peaks and deeps in time series of secondary cosmic rays, detected by surface particle detectors.

[5] Therefore the measurements of secondary fluxes can be used for "probing" ICMEs, providing highly cost-effective information on the key characteristics of these interplanetary disturbances. The size and magnetic field strength of ICMEs are correlated with the ICME modulation effects on the energy spectra and the direction of GCRs. At the same time the presence of a strong and long-duration southward magnetic field component in the sheath region of ICMEs is the primary requirement for their geoeffectiveness [*Valtonen*, 2007, and references therein]. Thus the strong magnetic field of the ICMEs is both a modulation agent of GCRs and a driver of geomagnetic storms (GMSs).

[1]Cosmic Ray Division, Yerevan Physics Institute, Yerevan, Armenia.

0148-0227/09/2009JA014346$09.00

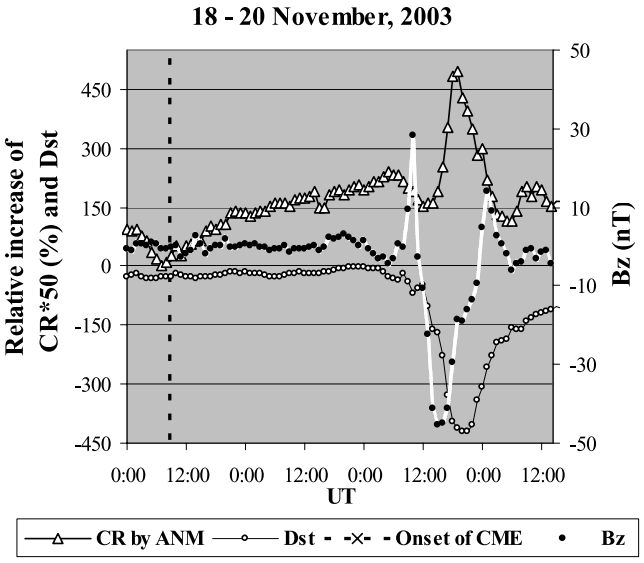

Figure 1. Coherent changes of the neutron flux intensity and *Dst* index. The B_z reaches its minimum 3 h earlier than the *Dst* minimum; note the pronounced peak in the neutron flux. CR intensity is multiplied by 50.

[6] Although there is no one-to-one dependence between the variations of the GCR and the strength of the GMS [see *Kudela and Brenkus*, 2004] and there exist other drivers of storms and modulation agents of GCRs, the large B_z value associated with approaching ICMEs is the best known diagnostic of GMS strength. Therefore appropriate observations of the variations of the primary and secondary cosmic rays can be a proxy of the B_z value available long before IMCEs reach the L1 libration point where B_z is measured directly [see, e.g., *Kudela and Storini*, 2006].

[7] The Solar and Heliospheric Observatory (SOHO) detected relativistic electrons with its Comprehensive Suprathermal and Energetic Particle Analyzer [*Müller-Mellin et al.*, 1995] instrument. Enhancements in the electron flux also can point to an approaching ICME. The modulation effects posed by ICMEs on the particles of higher energies, not measurable by space-borne facilities because of very weak fluxes, are detected by the world-wide networks of neutron monitors that respond to GCRs with rigidities of 1–14 GV and muon telescopes that respond to GCR rigidities of 2–100 GV well before the onset of a major geomagnetic storm [*Belov et al.*, 2003; *Munakata et al.*, 2000]. In addition, analysis of the correlation of the changes of cosmic ray fluxes in a large energy range with

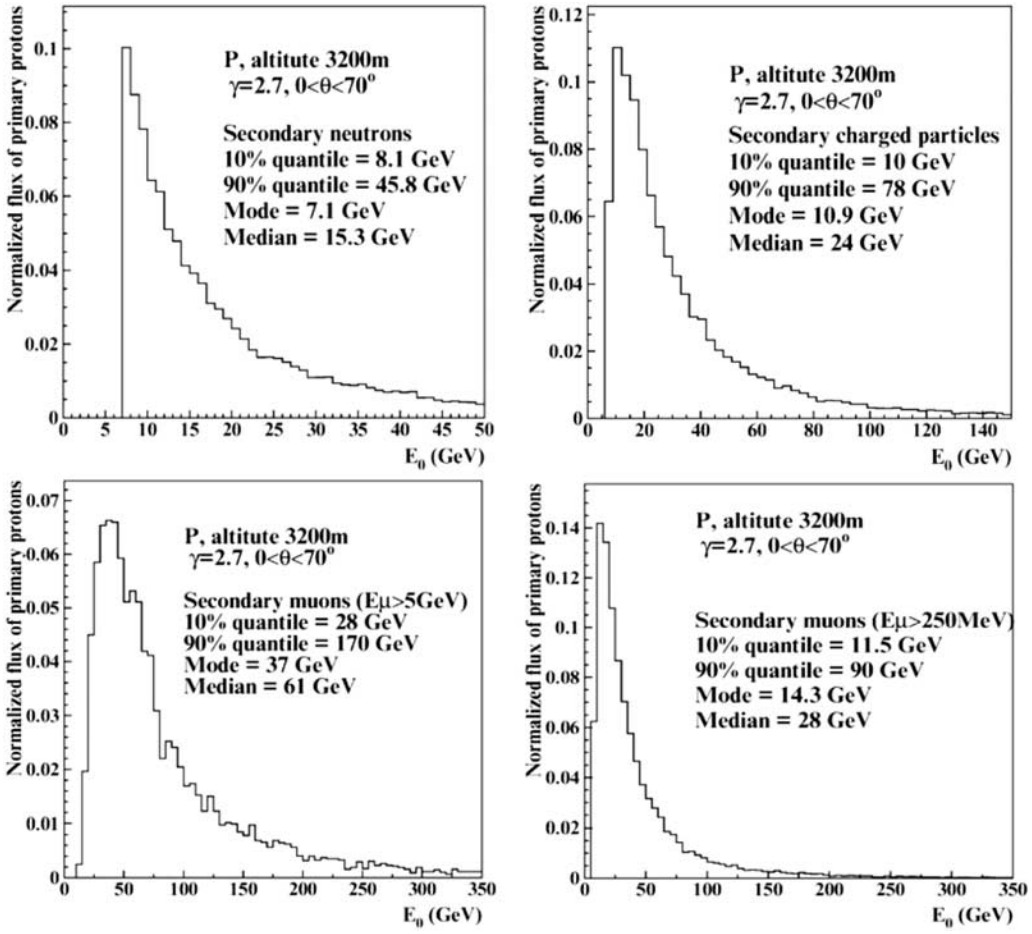

Figure 2. Energy distribution of the GCR protons initiated various secondary particles at Aragats at 3200-m altitude. The characteristics of the distributions (quantiles, mode, and median) help to estimate the most probable energy of each of the secondary particle species; the detection efficiency equals the ratio of primary protons to detected particles.

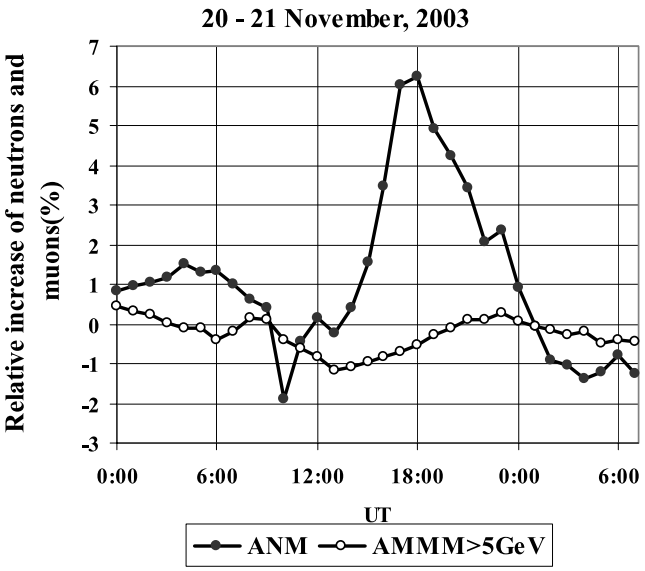

Figure 3. Changes of the hourly time series of Aragats Neutron Monitor (ANM) and Aragats Multichannel Muon Monitor (AMMM); no peak is detected in the >5 GeV muon flux.

geomagnetic effects makes it possible to check the development of the current system models in different stages of the geomagnetic storm [*Belov et al.*, 2005; *Kudela et al.*, 2008].

[8] GMSs usually lead to an increase in the intensity of secondary cosmic ray (CR) flux. In contrast to the modulation effects caused by other solar transient events (Forbush decreases and ground level enhancements), the GMS modulation effect is more pronounced at middle latitudes and not at high latitudes. The variety of particle detectors at the Aragats Space Environmental Center (ASEC) [*Chilingarian et al.*, 2003, 2005] allows us to extend the maximal energies from hundreds of MeV accessible to space-borne facilities up to tens of GeV. The aim of this paper is to get more insight into the correlation of IMCE parameters with geospace

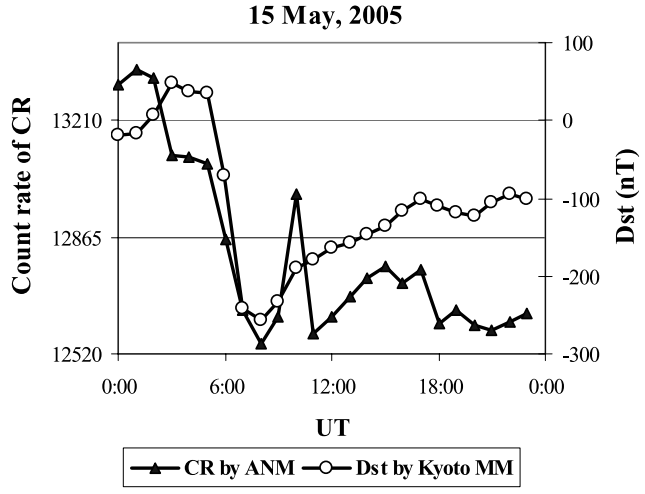

Figure 4. Hourly time series of Aragats Neutron Monitor count rate and the *Dst* index; uncorrelated changes.

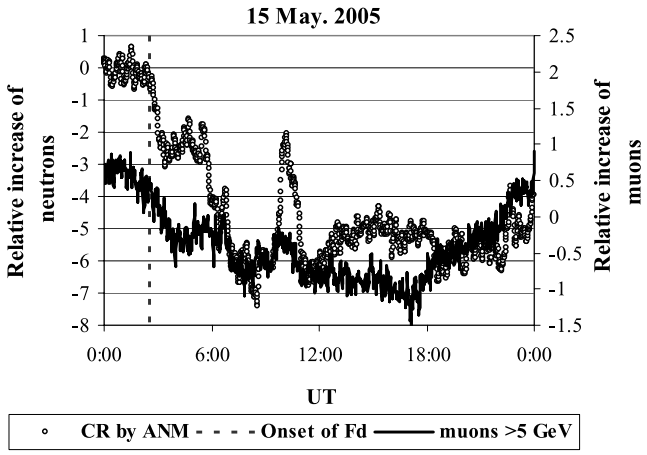

Figure 5. Time series of count rates of neutrons and >5 GeV muons demonstrate coherent peaks at an overall decrease in the cosmic ray intensity.

parameters, including the changing intensities of particle fluxes measured at the Earth's surface.

2. Selection of the Particle Events Related to the ICME-Induced Geomagnetic Effects

[9] Selection of the particle events related to geomagnetic storms was made by correlation analysis of the cosmic ray fluxes measured by the particle detectors operating at ASEC, the intensity of geomagnetic storms measured by magnetometers located at middle latitudes and summarized as the *Dst* index at the World Data Center for Geomagnetism, Kyoto, Japan (http://wdc.kugi.kyoto-u.ac.jp/dstdir/index.html), and B_z measurements in transient magnetic structures at their passage of the Advanced Composition Explorer (ACE) spacecraft (http://www.srl.caltech.edu/ACE/ASC/level2/lvl2DATA_MAG.html). The typical pattern of the intercorrelation of CR intensity, *Dst* index, and B_z is apparent in Figure 1. On 20 November 2003 a very large increase in CR intensity was detected by the Aragats Neutron Monitor (~7.5%) after a small Forbush decrease (FD). As we can see in Figure 1, the *Dst* index was decreasing, reaching a record value −472 nT, the severest GMS of cycle 23 [*Gopalswamy et al.*, 2005]. The correlation coefficient R between the 1-h time series of the *Dst* index and the neutron flux is −0.91 for the time span between 1400 UT on 20 November and 0500 UT on 21 November. Better anticorrelation (R = −0.96) is achieved with a 1-h shifted *Dst* time series taken from 1500 UT on 20 November to 0600 UT on 21 November). We also present in Figure 1 the most "geoeffective" ICME characteristic, B_z. The magnetic field of the ICME and geospace parameters (*Dst* and neutron flux, measured at the Earth surface) are well correlated; the approaching to Earth ICME influence the cosmic ray flux and unleash the geomagnetic storm. The B_z minimum (−48 nT), the CR intensity maximum, and the *Dst* minimum occur at 1630, 1900, and 2000 UT, respectively. The maximal "delayed" correlation (~2.5 h) between the CR intensity and B_z reaches −0.7.

[10] Coherent changes of CR intensity and *Dst* index pointed to the effective decrease of the strength of the

Table 1. Characteristics of Enhancements of the Neutral and Charged Secondary Cosmic Ray Fluxes During GMS and the Corresponding ICME and IMF Parameters As Well As Heliocoordinates of the CME Launch

Date	Heliocoordinates of CME	Increase of Neutron Count Rate (%)	Increase of Secondary Charged CR Count Rate (%)	*Dst* (nT)	B_z (nT)	Delay Times Between *Dst* and B_z Minimums (h)	Max. Speed of ICME (km/s)	Jump of V_{sw} (km/s)
2003.06.17	20°N, 70°E	0.5	na[a]	−21	−11	3	515	0
1999.09.15	7°S, 89°E	1.36	na[a]	−22	−12	1	615	105
1998.09.24	18°N, 14°E or20°S, 22°E	1.2	na[a]	−27	−9.4	5	520	70
1998.03.10	24°S, 67°W	0.97	na[a]	−28	−12	4.5	350	20
2000.08.10	?	1.1	na[a]	−29	−11	3.2	460	100
2003.06.17	?	1.4	0.68	−38	−12	2	535	0
2004.11.09	9°N, 17°W	1.6	0.65	−66	−14.8	2	695	118
1998.03.21	?	2.6	na[a]	−76	−23	2.3	600	180
2004.11.07	8°N,15°E	1.9	na[a]	−80	−20	3	688	214
2000.08.11	22°N, 71°W	1.4	na[a]	−81	−20	6	440	0
2003.06.18	7°S, 80°E	4	na[a]	−107	−22	3.5	556	100
2002.09.07	9°N, 28°W	2.3	1	−112	−25	2.5	570	180
1998.08.06	19°S, 78°E	2.3	na[a]	−115	−21	3	430	60
1999.10.22	?	2.6	na[a]	−128	−21	3	690	195
1998.05.04	15°S, 15°W	3.1	na[a]	−143	−26	2	860	380
1998.09.25	18°N, 9°E	3.5	na[a]	−166	−36	2.5	830	400
1999.09.23	21°N, 76°W	3.7	na[a]	−191	−38	3.2	600	245
2000.08.12	11°N, 11°W	3.7	na[a]	−205	−40	2.5	670	250
2005.08.24	?	3.64	1.4	−216	−49	1.5	750	200
2003.10.30	15°S, 02°W	4.1	1.7	−283	−36	2.5	>1000[b]	
2003.10.29	16°S, 8°E	5.6	2	−320	−41	5	>1000[b]	
2004.11.08	10°N, 8°E	5.9	2.2	−413	−45	4	814	340
2001.03.31	20°N, 19°W	6	na[a]	−415	−48	2.3	770	330
2003.11.20	0°N, 18°E	7.5	3	−455	−49	4	770	325
2003.06.17	20°N, 70°E	0.5	na[a]	−21	−11	3	515	0
1999.09.15	7°S, 89°E	1.36	na[a]	−22	−12	1	615	105
1998.09.24	18°N, 14°E or 20°S, 22°E	1.2	na[a]	−27	−9.4	5	520	70
1998.03.10	24°S, 67°W	0.97	na[a]	−28	−12	4.5	350	20
2000.08.10	?	1.1	na[a]	−29	−11	3.2	460	100
2003.06.17	?	1.4	0.68	−38	−12	2	535	0
2004.11.09	9°N, 17°W	1.6	0.65	−66	−14.8	2	695	118
1998.03.21	?	2.6	na[a]	−76	−23	2.3	600	180
2004.11.07	8°N, 15°E	1.9	na[a]	−80	−20	3	688	214
2000.08.11	22°N, 7°W	1.4	na[a]	−81	−20	6	440	0
2003.06.18	7°S, 80°E	4	na[a]	−107	−22	3.5	556	100
2002.09.07	9°N,28°W	2.3	1	−112	−25	2.5	570	180
1998.08.06	19°S, 78°E	2.3	na[a]	−115	−21	3	430	60
1999.10.22	?	2.6	na[a]	−128	−21	3	690	195
1998.05.04	15°S, 15°W	3.1	na[a]	−143	−26	2	860	380
1998.09.25	18°N, 09°E	3.5	na[a]	−166	−36	2.5	830	400
1999.09.23	21°N, 76°W	3.7	na[a]	−191	−38	3.2	600	245
2000.08.12	11°N, 11°W	3.7	na[a]	−205	−40	2.5	670	250
2005.08.24	?	3.64	1.4	−216	−49	1.5	750	200
2003.10.30	15°S, 2°W	4.1	1.7	−283	−36	2.5	>1000[b]	
2003.10.29	16°S, 08°E	5.6	2	−320	−41	5	>1000[b]	
2004.11.08	10°N, 08°E	5.9	2.2	−413	−45	4	814	340
2001.03.31	20°N, 19°W	6	na[a]	−415	−48	2.3	770	330
2003.11.20	0°N, 18°E	7.5	3	−455	−49	4	770	325

[a]No ASEC data were available.
[b]On 29 and 30 October 2003 the ACE solar wind detector was put in standby mode and the SOHO detector was saturated.

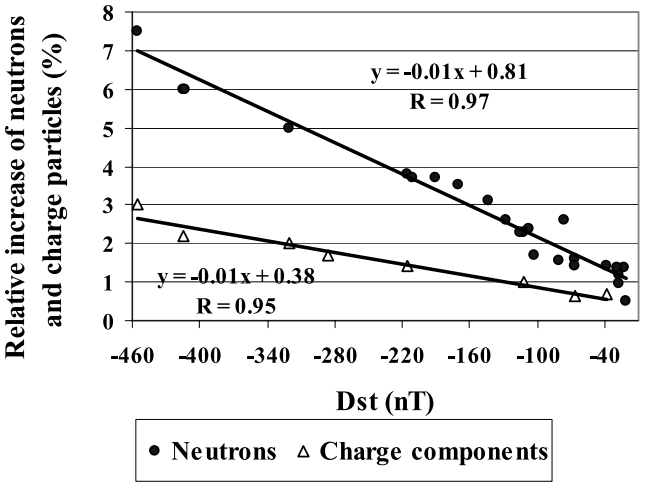

Figure 6. Relation between relative increase of charged and neutral components during the GMS and the corresponding values of the *Dst* index.

geomagnetic field because of its coupling with the ICME magnetic field. As we mentioned in section 1, such effects were triggered by ICMEs with strong southward magnetic fields. A decrease in cutoff rigidity will allow primary protons and nuclei (with energies lower than usual) to enter the atmosphere and generate particle cascades reaching the Earth's surface, thus increasing the count rate of particle detectors. However, not all secondary fluxes will be enhanced. In Figure 2 the energy distributions of the primary protons, which generated neutrons and low- and high-energy muons, are depicted. Primary protons with energies immediately contiguous the ones corresponding to the cutoff can generate secondary neutrons; in contrast, the $\geq$5 GeV muons can be generated only by primary protons with energies $\geq$15 GeV [see also *Wang and Wang*, 2006a]. Therefore the flux of high-energy muons detected by the Aragats Multichannel Muon Monitor during 20–21 November, as we can see in Figure 3, remains unchanged during the severe disturbance of the magnetosphere. The decrease in the cutoff rigidity cannot influence the $\geq$5 GeV muon flux because the primary protons have much more energy than those corresponding to the rigidity cutoff.

[11] In Figure 4 we can see another kind of neutron intensity enhancement not correlated with the sudden commencement of a geomagnetic storm. On 15 May 2005, after the large FD, we detected a 4.3% enhancement of the Aragats Neutron Monitor count rate, but the delay of the flux maximum compared with the observed minimum of *Dst* was approximately 3 h. Furthermore, the 5 GeV muons also demonstrate the peak apparent in Figure 5; thus the interplanetary magnetic field (IMF) or/and system of magnetospheric currents were highly disturbed, enabling an additional portion of the high-energy primary protons to enter the atmosphere.

[12] Examining all cases of coherent changes of count rate and *Dst* index, we selected 24 GMS events (for 8 of which we also have time series of low- and high-energy muons). Characteristics of these events are listed in the Table 1; events are arranged in ascending order of GMS severity measured by *Dst* index.

[13] Characteristics of the CMEs are from the Master Data Table of Major Geomagnetic Storms (1996–2005) (http://cdaw.gsfc.nasa.gov/geomag_cdaw/Data_master_table.html); increases in neutral and charged cosmic ray species are measured during GMSs by ASEC particle detectors; the *Dst* index is taken from the World Data Center for Geomagnetism, Kyoto, Japan (http://wdc.kugi.kyoto-u.ac.jp/dstdir/index.html); B_z is measured in transient magnetic structures at their passage of the ACE spacecraft (http://www.srl.caltech.edu/ACE/ASC/level2/lvl2DATA_MAG.html); and maximal speed of solar wind (V_{sw}) and jump of the V_{sw} are estimated by data from facilities of ACE spacecraft. We calculate the delay time of the *Dst* minimum relative to the B_z minimum, and the average time of this delay is equal to $\sim$3 h.

3. Correlations Between the Level of Increase of CR Intensity and the Severity of the GMS

[14] In Table 1 we present the parameters of a disturbed IMF: the southward component of magnetic field B_z and the change of the V_{sw} at the magnetic cloud-shock transition measured by SOHO and ACE spacecrafts. Coherently changing geophysical parameters measured by the surface magnetometers and networks of particle detectors are also listed in Table 1. Clearly, the common driver of all the changes is the ICME, and the most geoeffective parameters of the ICME are the strength, direction, size, and velocity of the magnetic field.

[15] In Figure 6 we can see that the CR increase (both neutrons and low-energy charged particles) and GMS severity are well correlated to the GMS events of the 23rd cycle (correlation coefficients are 0.97 and 0.95 for the neutrons and charged components, respectively). A similar relationship was obtained for the B_z, measured at ACE, and the particle flux enhancement measured by the ASEC monitors (see Figure 7). It is evident that both the cosmic ray intensity changes and the strength of the geomagnetic storm are determined by one and the same ICME parameter, namely, B_z.

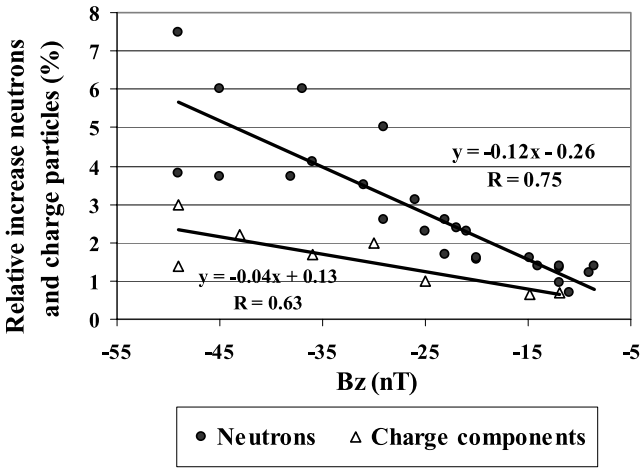

Figure 7. Relation between the relative increase of cosmic ray intensity (neutrons and charge components) and B_z.

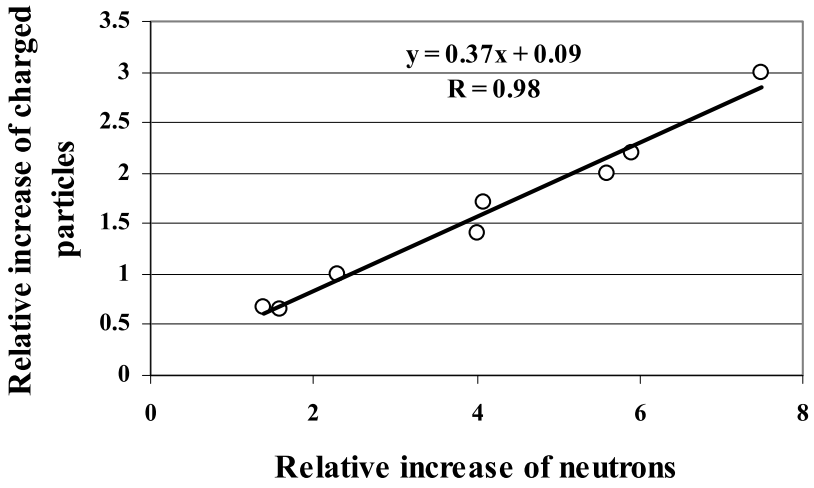

Figure 8. Relation between the relative increases of neutral and charged components of secondary CRs during GMSs.

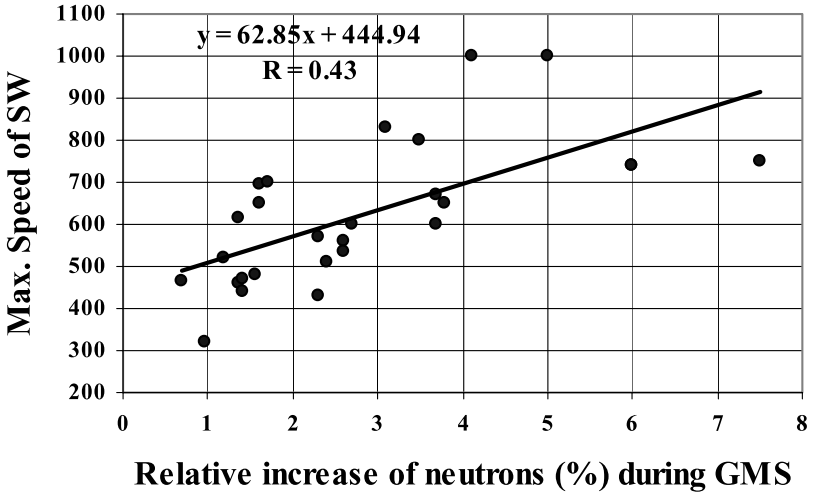

Figure 9. Dependence of the maximal value of solar wind speed V_{sw} on the relative increase of the CR count rate for events listed in Table 1.

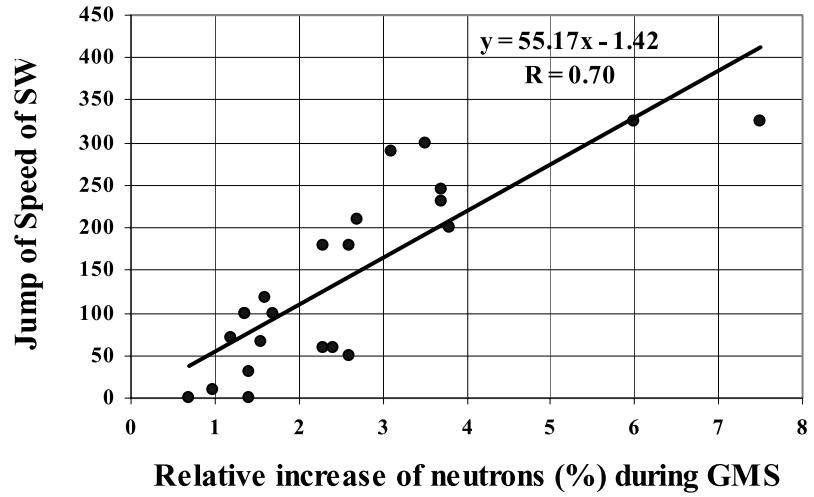

Figure 10. Dependence of the solar wind speed jump on the relative increase of the CR count rate.

Table 2. Relative Increase of the Neutron Monitor Count Rate During GMS

Category of Storm (nT)	*Dst* (nT)	B_z (nT)	Relative Increase of Neutrons (%)	Jump of V_{sw} (km/s)
Weak (−30 to 50)	−28	−11	1.0	52
Moderate (−50 to 100)	−76	−20	1.9	128
Strong (−100 to 200)	−121	−27	3.1	215
Severe (−200 to 350)	−200	−33	4.0	250
Great (<−350)	−428	−48	6.5	330

[16] As we can see from Figures 6, 7, and 8, the increases of the flux of different CR species are highly correlated, and the increase of neutrons is always greater than the increase of low-energy charged particles. The difference in peak amplitudes can be explained by the fact that lower-energy primary particles produce neutrons in contrast to the primaries that generate electrons and muons reaching the Earth's surface (see Figure 2). Detailed information on the distributions of primaries is given by *Chilingarian and Zazyan* [2009].

[17] It has been demonstrated that ~70% of all front-side high-speed halo CMEs are geoeffective [*Gopalswamy et al.*, 2007; *Wang and Wang*, 2006b]. Therefore halo CMEs provide a warning of the imminent danger tens of hours before CMEs reach 1 AU and unleash geomagnetic storms. By measuring the magnitude of the southward magnetic field at 1 AU (or at the libration point L1), it is possible also to forecast the strength of the expected geomagnetic storm (see Figure 1). Using the ICME parameters measured by ACE spacecraft, several groups are providing short-term forecasts of the strength of the expected geomagnetic storm [see, e.g., *Li et al.*, 2007]. Information on the changing cosmic ray fluxes also can be very useful, especially when space-borne facilities are put in the standby mode because of abundant cosmic ray fluxes and when ground-based data are online.

[18] In addition to the B_z, solar wind speed can be used for forecasting the severity of upcoming GMSs. In Figures 9 and 10 we present dependence of the peak increase of secondary cosmic ray flux on the solar wind speed and on the "jump" in the solar wind speed at the shock transition. As has been previously mentioned [see, e.g., *Kane*, 2006], the linear correlation of solar wind parameters with CR flux relative increase is weaker than the B_z dependence. From Figures 9 and 10 we can conclude that the changes of cosmic ray fluxes (which we use as a proxy for the GMS severity) better correlate with the changes of the solar wind speed (jump) at L1 point than with the maximal speed of the solar wind.

[19] In Table 2 we combine 24 events in five groups according to the GMS severity, as proposed by *Loewe and Prolss* [1997]; the values posted in the columns of Table 2 are group averages of geospace parameters. It is interesting to note that the quadratic function describes the data very precisely (see Figure 11; in contradiction to the common view that the solar wind speed correlates poorly with *Dst* [see, e.g., *Kane*, 2006]). This contradiction points out the limitations of the linear correlation analysis and the rather strong influence of groupings of the GMS data.

4. ICME Arrival at 1 AU and Cosmic Ray Intensity Changes

[20] The time series of the cosmic ray intensities are closely related to the magnetic properties and the structure of the approaching ICME [*Bieber and Evenson*, 1998]. Using the model of the inclined cylinder to represent a large-scale loop structure draped from the Sun by a CME, *Kuwabara et al.* [2004] derived the three-dimensional geometry of the cosmic ray depleted region behind the shock. GMS events of the 23rd solar cycle give several examples of the various patterns of ICME interactions with magnetosphere (see discussion by *Wang* [2007]). If we accept the inclined cylinder geometry with slow rotation of the magnetic field, different patterns of the secondary flux enhancement should arise. If the B_z is southward just at the arrival of the ICME, the cosmic ray flux will show a peak coinciding in time (or tens of minutes later) with the abrupt change of the solar wind speed and B_z measured by ACE (see Figure 12). The change of the effective cutoff rigidity due to the reduction of the geomagnetic field lasting

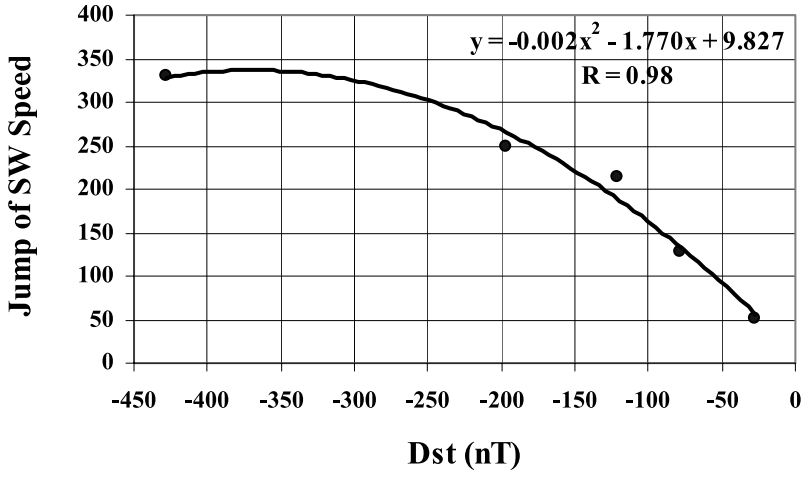

Figure 11. The same dependence as in Figure 10, with the data from Table 2 grouped in five GMS categories.

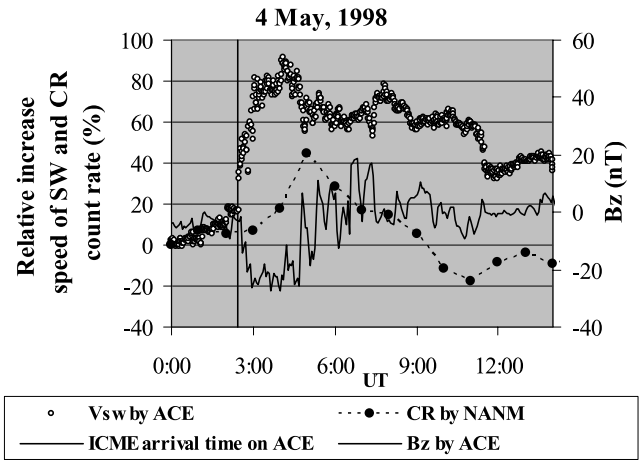

Figure 12. The ICME arrives at 1 AU with a southward oriented B_z component of the magnetic field. Observed cosmic ray intensity enhancement is followed by a Forbush decrease.

several hours allows the lower-energy primary GCRs to enter the atmosphere and generate particle cascades detected by the particle monitors located at the Earth's surface. After the passage of the ICME the disturbed geomagnetic field is recovered and again prevents the low-energy particle from entering the atmosphere. Furthermore, the overall disturbance of the IMF leads to an overall depletion of the cosmic ray intensity (the so-called Forbush decrease), starting just after the end of the geomagnetic storm (see Figure 12).

[21] If the magnetic field at the arrival of the ICME is not oriented southward, we detect first a Forbush decrease followed after several hours by an increase of CR intensity (see Figure 13). In Figure 13 we can see that on 20 November 2003 the B_z becomes southward only 5 h after the interaction of the ICME with the magnetosphere. At the same time we detect the start of the CR flux intensity increase.

5. Conclusion

[22] Severe geomagnetic storms are known to be triggered by prolonged periods of negative B_z (when the latter reconnects with the terrestrial magnetic field); thus the *Dst* index can be predicted from the solar wind and interplanetary magnetic field conditions. The cosmic ray flux also changes because of approaching ICMEs. Therefore the changing fluxes of secondary cosmic rays measured at the Earth's surface can be used as proxies of ICME parameters when measurements at L1 Lagrange point are not feasible because of severe radiation storms.

[23] Information on the simultaneous detection of GMS in neutral and charged fluxes gives clues on the disturbance of the IMF and the magnetosphere. The ratio between increases of neutral and charged fluxes is approximately constant in a large range of GMS severity, and neutral flux always undergoes larger changes than the charged component.

[24] The linear correlation of solar wind parameters with the CR flux relative increase is weaker than the B_z dependence. The maximal enhancement of the neutron flux during the GMS was ~7.5% and that of the low-energy

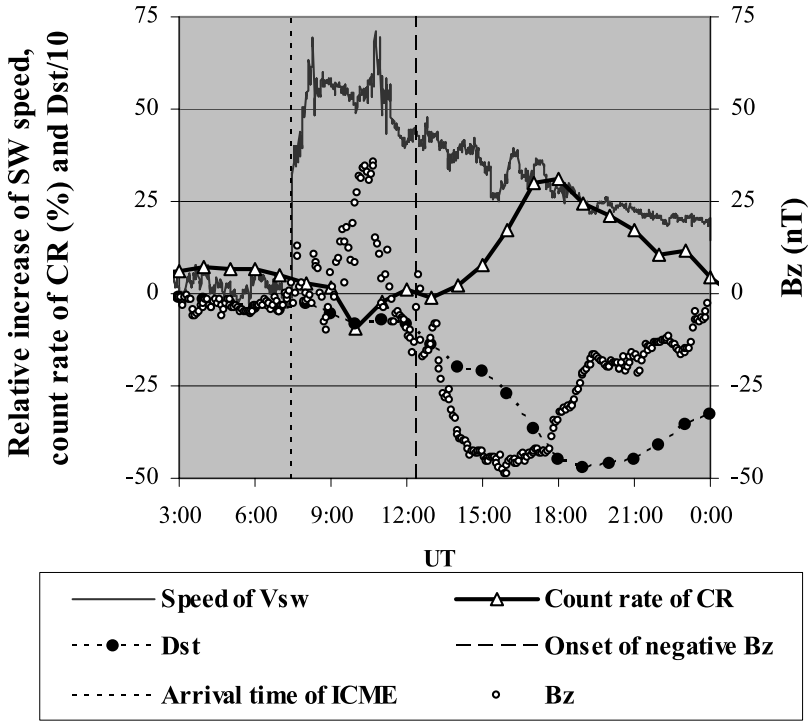

Figure 13. The B_z at the arrival of the ICME is not oriented southward. We detect first a Forbush decrease followed after several hours by an intensity increase of the CR (when the B_z component of magnetic field comes to be southward).

charged particles was ~3% during the 23rd solar cycle according to data collected by particle detectors of the Aragats Space Environmental Center. The relative time of successive changes of CR flux intensity increases (because of geomagnetic storm) and intensity decreases (Forbush decreases) can be used for the determination of the ICME structure.

[25] **Acknowledgments.** This work was partly supported by ISTC A1554 grant and INTAS 8777 grant. The authors thank N. Gopalswamy and G. Karapetyan for useful discussions and the ASEC staff for providing continuous operation of the particle detectors during the 23rd solar activity cycle.

[26] Amitava Bhattacharjee thanks the reviewers for their assistance in evaluating this paper.

References

Belov, A. V., J. W. Bieber, E. A. Eroshenko, P. Evensong, R. Pyle, and V. G. Yankee (2003), Cosmic ray anisotropy before and during the passage of major solar wind disturbances, *Adv. Space Res.*, *31*, 919–924, doi:10.1016/S0273-1177(02)00803-7.

Belov, A., L. Baisultanova, E. Eroshenko, H. Mavromichalaki, V. Yanke, V. Pchelkin, C. Plainaki, and G. Mariatos (2005), Magnetospheric effects in cosmic rays during the unique magnetic storm on November 2003, *J. Geophys. Res.*, *110*, A09S20, doi:10.1029/2005JA011067.

Bieber, J. W., and P. Evenson (1998), CME geometry in relation to cosmic ray anisotropy, *Geophys. Res. Lett.*, *25*, 2955–2958, doi:10.1029/98GL51232.

Chilingarian, A., and M. Zazyan (2009), Calculations of the sensitivity of the particle detectors of ASEC and SEVAN networks to galactic and solar cosmic rays, *Astropart. Phys.*, doi:10.1016/j.astropartphys.2009.08.001, in press.

Chilingarian, A., et al. (2003), Aragats Space–Environmental Center: Status and SEP forecasting possibilities, *J. Phys. G Nucl. Part. Phys.*, *29*, 939–952, doi:10.1088/0954-3899/29/5/314.

Chilingarian, A., et al. (2005), Correlated measurements of secondary cosmic ray fluxes by the Aragats Space–Environmental Center monitors, *Nucl. Instrum. Methods Phys. Res., Sect. A*, *543*, 483–496, doi:10.1016/j.nima.2004.12.021.

Dvornikov, V. M., V. E. Sdobnov, and A. V. Sergeev (1988), Anomalous variations of cosmic rays in the rigidity range of 2–5 GV and their connection with heliospheric disturbances (in Russian), *Akad. Nauk SSSR Izvestiia Ser. Fizicheskaia*, *52*, 2435–2437.

Gopalswamy, N., S. Yashiro, G. Michalek, H. Xie, R. P. Lepping, and R. A. Howard (2005), Solar source of the largest geomagnetic storm of cycle 23, *Geophys. Res. Lett.*, *32*, L12S09, doi:10.1029/2004GL021639.

Gopalswamy, N., S. Yashiro, and S. Akiyama (2007), Geoeffectiveness of halo coronal mass ejections, *J. Geophys. Res.*, *112*, A06112, doi:10.1029/2006JA012149.

Kane, R. P. (2006), Cosmic ray anisotropies around the Forbush decrease of April 11, 2001, *Sol. Phys.*, *234*, 353–362, doi:10.1007/s11207-006-0083-8.

Koskinen, H. E. J., and K. M. J. Huttunen (2006), Space weather:from solar eruptions to magnetospheric storms, in *Solar Eruptions and Energetic Particles*, *Geophys. Monogr. Ser.*, vol. 165, edited by N. Gopalswamy, R. Mewaldt, and J. Torsti, pp. 375–385, AGU, Washington, D. C.

Kudela, K., and R. Brenkus (2004), Cosmic ray decreases and geomagnetic activity: List of events 1982–2002, *J. Atmos. Sol. Terr. Phys.*, *66*, 1121–1126.

Kudela, K., and M. Storini (2006), Possible tools for space weather issues from cosmic ray continuous records, *Adv. Space Res.*, *37*, 1443–1449, doi:10.1016/j.asr.2006.02.058.

Kudela, K., R. Buchık, and P. Bobık (2008), On transmissivity of low energy cosmic rays in disturbed magnetosphere, *Adv. Space Res.*, *42*, 1300–1306, doi:10.1016/j.asr.2007.09.033.

Kuwabara, T., et al. (2004), Geometry of an interplanetary CME on October 29, 2003, deduced from cosmic rays, *Geophys. Res. Lett.*, *31*, L19803, doi:10.1029/2004GL020803.

Li, X., K. S. Oh, and M. Temerin (2007), Prediction of the AL index using solar wind parameters, *J. Geophys. Res.*, *112*, A06224, doi:10.1029/2006JA011918.

Loewe, C. A., and G. W. Prolss (1997), Classification and mean behavior of magnetic storms, *J. Geophys. Res.*, *102*, 14,209–14,213, doi:10.1029/96JA04020.

Müller-Mellin, R., et al. (1995), COSTEP—Comprehensive Suprathermal and Energetic Particle Analyser, *Sol. Phys.*, *162*, 483–504, doi:10.1007/BF00733437.

Munakata, K., J. W. Bieber, S. Yasue, C. Kato, M. Koyama, S. Akahane, K. Fujimoto, Z. Fujii, J. E. Humble, and M. L. Duldig (2000), Precursors of geomagnetic storms observed by the muon detector network, *J. Geophys. Res.*, *105*, 27,457–27,468, doi:10.1029/2000JA000064.

Valtonen, E. (2007), Geoeffective coronal mass ejections and energetic particles, in *Solar Eruptions and Energetic Particle*, *Geophys. Monogr. Ser.*, vol. 165, edited by N. Gopalswamy, R. Mewaldt, and J. Torsti, pp. 335–344, AGU, Washington, D. C.

Wang, R. (2007), Large geomagnetic storms of extreme solar event periods in solar cycle 23, *Adv. Space Res.*, *40*, 1835–1841, doi:10.1016/j.asr.2007.03.015.

Wang, R., and J. Wang (2006a), Spectra and solar energetic protons over 20 GeV in Bastille Day event 25, *Astropart. Phys.*, *25*, 41–46, doi:10.1016/j.astropartphys.2005.11.002.

Wang, R., and J. Wang (2006b), Investigation of the cosmic ray ground level enhancements during solar cycle 23, *Adv. Space Res.*, *38*, 489–492, doi:10.1016/j.asr.2005.03.059.

N. Bostanjyan and A. Chilingarian, Cosmic Ray Division, Yerevan Physics Institute, Alikhanyan Brothers 2, Yerevan 36, Armenia. (nikolai@yerphi.am)